Submitted to ApJ
Preprint typeset using LaTeX style emulateapj v. 10/09/06

DELVING DEEPER INTO THE TUMULTUOUS LIVES OF GALACTIC DWARFS: MODELING STAR FORMATION HISTORIES

Chris Orban[1,2], Oleg Y. Gnedin[3], Daniel R. Weisz[4], Evan D. Skillman[4], Andrew E. Dolphin[5], and Jon A. Holtzman[6]

(Dated: July 2, 2008)
Submitted to ApJ

ABSTRACT

The paucity of observed dwarf galaxies in the Local Group relative to the abundance of predicted dark matter halos remains one of the greatest puzzles of the ΛCDM paradigm. Solving this puzzle now requires not only matching the numbers of objects but also understanding the details of their star formation histories. We present a summary of such histories derived from the HST data using the color-magnitude diagram fitting method. To reduce observational uncertainties, we condense the data into five cumulative parameters – the fractions of stellar mass formed in the last 1, 2, 5, and 10 Gyr, and the mean stellar age. We interpret the new data with a phenomenological model based on the mass assembly histories of dark matter halos and the Schmidt law of star formation. The model correctly predicts the radial distribution of the dwarfs and the fractions of stars formed in the last 5 and 10 Gyr. However, in order to be consistent with the observations, the model requires a significant amount of recent star formation in the last 2 Gyr. Within the framework of our model, this prolonged star formation can be achieved by adding a stochastic variation in the density threshold of the star formation law. The model results are not sensitive to late gas accretion, the slope of the Schmidt law, or the details of cosmic reionization. A few discrepancies still remain: our model typically predicts too large stellar masses, only a modest population of ultra-faint dwarfs, and a small number of dwarfs with anomalously young stellar populations. Nevertheless, the observed star formation histories of Local Group dwarfs are generally consistent the expected star formation in cold dark matter halos.

Subject headings: cosmology: theory — galaxies: formation — galaxies: dwarf

1. INTRODUCTION

The discrepancy between the number of observed dwarf satellite galaxies of the Milky Way and the anticipated number of dark matter halos in cosmological simulations has been heralded as the "missing satellite problem" (Klypin et al. 1999; Moore et al. 1999; Kauffmann et al. 1993) and it still remains one of the greatest puzzles of the ΛCDM paradigm. One class of suggested solutions to this puzzle involves modifications to the nature of dark matter (e.g., Spergel & Steinhardt 2000) or to the initial conditions of cosmic structure (e.g., Zentner & Bullock 2003a,b; Kamionkowski & Liddle 2000; Colín et al. 2000), while another class of solutions invokes astrophysical arguments such as inefficient cooling of cosmic gas and/or feedback from young stars (e.g. Thoul & Weinberg 1996; Dekel & Woo 2003).

Motivated by this latter class of solutions, Kravtsov, Gnedin, & Klypin (2004, hereafter referred to as KGK04) developed a star formation model for the satellite galaxies, based on the mass assembly histories of individual dark matter halos in a ΛCDM cosmological simulation. That model incorporated the accretion of gas in hierarchical mergers and the loss of gas caused by the extragalactic UV background, and included both a continuous mode and a starburst mode of star formation. The model correctly reproduced the observed number of satellites of the Milky Way and M31, the radial distribution of luminous satellites, and the morphological segregation of dwarf irregular (dIrr) and dwarf spheroidal (dSph) galaxies. Recent N-body simulations of Madau et al. (2008), with the updated WMAP3 cosmological parameters, have confirmed the qualitative picture of KGK04.

The amount of observational data for Local Group dwarfs has been increasing steadily in the last several years, shifting the focus from simply counting the number of dwarf galaxies to deriving their detailed star formation histories (SFHs). Most Local Group dwarfs have now been observed with the *HST*, which has provided color-magnitude diagrams of resolved stellar populations in single or multiple fields (Dolphin et al. 2005; Holtzman et al. 2006). We parametrize these data as the fractions of stars formed in the last 1 Gyr, 2 Gyr, 5 Gyr, and 10 Gyr, and present these fractions in our Table 1. The data show a great variety of star formation histories – some continuous, some bursty, some truncated. In this paper we extend the model of KGK04 to account for such varied histories of the Local Group dwarfs and argue that adding a stochastic threshold to the star formation law greatly improves the comparison between models and observations. We also make predictions for the number of ultra-faint satellites of the Milky Way and M31 of which there have been many recent discoveries with

[1] Center for Cosmology and Astro-Particle Physics, The Ohio State University, 191 W Woodruff Ave, Columbus, OH 43210
[2] Department of Physics, The Ohio State University, 191 W Woodruff Ave, Columbus, OH 43210; orban@mps.ohio-state.edu
[3] Department of Astronomy, University of Michigan, 500 Church St., Ann Arbor, MI 48109; ognedin@umich.edu
[4] Department of Astronomy, University of Minnesota, 116 Church St. SE, Minneapolis, MN 55455
[5] Raytheon Corporation, USA
[6] Astronomy Department New Mexico State University, Box 30001, MSC 4500 Las Cruces, NM 88003

the Sloan Digital Sky Survey (SDSS) and the MegaCam survey (Belokurov et al. 2006, 2007; Irwin et al. 2007; Liu et al. 2008; Martin et al. 2006; Simon & Geha 2007; Walsh et al. 2007; Willman et al. 2005a,b; Zucker et al. 2004, 2006a,b, 2007).

Our approach is complementary to running full hydrodynamic simulations of galaxy formation. We attempt to model star formation with a phenomenological recipe, containing several but not too many free parameters. We investigate the effects of varying each of these parameters and constrain them by comparing the model predictions for each parameter set with the observations. In this way, we obtain empirical rules that govern star formation in dwarf galaxies, even though we may not yet fully understand their physical origin. In an alternative approach, one uses cosmological hydrodynamic simulations with a detailed prescription for gas cooling and star formation, and thus obtains more physically sound results. Discrepancies between the simulation results and the data may, however, be difficult to interpret or computationally expensive to investigate. By combining the two approaches, our empirical rules will guide future developments of more sophisticated models of galaxy formation.

The paper is organized as follows. We give a brief summary of the observational data in §2. We describe our model in §3 and report the primary results from adding stochasticity to the star formation law in §4. In §5 we describe the results of several variants of our star formation model, including late accretion of gas, steeper slopes of the Schmidt law, an extended epoch of reionization, and rejection of galaxies with delayed star formation; none of these changes significantly alters our results. In §6 we show our model projections for the new low-mass dwarfs, and in §7 we summarize our main results.

2. OBSERVED STAR FORMATION HISTORIES

The star formation data used in this study, and listed in Table 1, come primarily from Hubble Space Telescope observations with the WFPC2 camera. For a majority of the dwarfs, the SFHs were measured by the color-magnitude diagram fitting method, described in Dolphin (2002), using photometric data from the Local Group Stellar Photometry Archive[1] (Holtzman et al. 2006). We condense the data into five parameters – the fractions of stellar mass formed in the last 1, 2, 5, and 10 Gyr, respectively (f_{1G}, f_{2G}, f_{5G}, f_{10G}), and the mass-weighted mean age of the stellar population (τ). The HST observations included in archive are far from homogeneous, and, therefore, the uncertainties in the derived star formation histories cover a broad range. However, by concentrating on cumulative star formation fractions the uncertainties are greatly reduced, compared to specific star formation rates at specific times. Thus, the entries in Table 1 do not have associated errors. Constraining comparisons between models and observations to cumulative distributions greatly reduces the sensitivity of these comparisons to uncertainties in individual galaxies.

Note that the observed *HST* fields do not necessarily cover the full extent of each galaxy and, therefore, do not allow us to calculate the total stellar mass. For the estimate of total stellar mass, with a few exceptions, we take the values quoted in Dekel & Woo (2003).

[1] http://astronomy.nmsu.edu/holtz/archival/html/lg.html

The rest of the SFHs are taken from a variety of sources, as indicated in the notes to Table 1. In the case of the LMC, the star formation data are inferred from Smecker-Hane et al. (2002). Since they give the star formation rates per unit area, in units of $M_\odot\,yr^{-1}\,deg^{-2}$, separately for the disk and the bar of the LMC, we assume that the extent of the disk is 3.5 times larger than the extent of the bar in determining the star formation fractions and the mean age (A. A. Cole, personal communication).

The star formation histories for five dwarfs (M32, M33, Antlia, Sextans, Ursa Minor) are taken from Table 1 of Dolphin et al. (2005). Since that table does not include the fraction of a galaxy's star formation in the last 2 Gyr or 5 Gyr, our table is also missing these entries, except for Sextans and Ursa Minor. Dolphin et al. (2005) reported that Sextans and Ursa Minor have formed no stars in the past 10 Gyr (i.e., $f_{10G} = 0$), which implies that the fractions of stars formed in the last 1 Gyr, 2 Gyr, and 5 Gyr are also consistent with zero.

For the purpose of comparing the radial distributions of different morphological types with model predictions, we combine the Sc, Irr, and dIrr types into one broadly-defined "dIrr" group, and the dE, dSph types into the "dSph" group.

One object not included in Table 1 is the Canis Major dwarf, discovered by Martin et al. (2004) in the SDSS field, which could be part of a larger Monoceros tidal stream. This object is the closest discovered to the Galaxy, at a heliocentric distance of only 8 kpc. Whether this galaxy is still gravitationally self-bound is unclear at present (Butler et al. 2007), but in any case it is being strongly tidally disrupted. An additional reason for not including it in our comparison is that such an object would have been completely disrupted in the N-body numerical simulation used to construct our models.

Note also that Table 1 does not include any of the newly-discovered SDSS and MegaCam ultrafaint dwarfs, since they are likely to have stellar masses below 5×10^5 $M_\odot$. We list these new objects in Table 8 and compare their estimated stellar mass function with the predictions of our fiducial model in §6.

3. STAR FORMATION MODEL

The KGK04 model of star formation in dwarf galaxies is based on the mass assembly history of dark matter halos in a collisionless ΛCDM simulation of the Local Group-like environment. The simulation volume contains three large host halos, with virial masses $(1.2 - 1.7) \times 10^{12}\ h^{-1}\ M_\odot$ at $z = 0$, resolved with $\sim 10^6$ dark matter particles. The model incorporates the accretion of gas in hierarchical mergers and the loss of gas caused by the extragalactic UV background (following the filtering mass approach of Gnedin 2000), and includes both a continuous mode and a starburst mode of star formation.

The model assumes that in the satellite halos the accreted gas dissipates its energy via radiative cooling and forms a disk. The surface density of the gas follows an exponential profile,

$$\Sigma_g(r) = \Sigma_0 \exp\left(-r/r_d\right), \tag{1}$$

with the scale length r_d set by the satellite halo's virial radius $r_{\rm vir}$ and angular spin parameter λ:

$$r_d = \lambda\, r_{\rm vir}\, 2^{-1/2}\, \exp\left[c(V_4/V_{\rm max})^2\right]. \tag{2}$$

TABLE 1
Star Formation Histories of Satellite Galaxies of MW and M31

Galaxy	Alternate Name	Type	Host	$r_{\rm host}$ (kpc)	$\log(M_{*,\odot})$	f_{1G}	f_{2G}	f_{5G}	f_{10G}	τ (Gyr)
M33	NGC598	Sc	M31	203	9.9	0.093			0.52	8.4
LMC		Irr	MW	50	9.7	0.078	0.17	0.42	0.70	6.7
SMC		Irr	MW	63	9.2	0.096	0.18	0.48	0.65	6.6
M32	NGC221	dE	M31	6	9.1	0.042			0.50	8.5
NGC205	M110	dE	M31	58	9.0	0.0049	0.0050	0.055	0.48	10.5
IC10		dIrr	M31	255	8.7	0.060	0.14	0.52	0.75	7.1
NGC6822		dIrr	MW	500	8.7	0.087	0.16	0.57	0.68	6.9
NGC3109		dIrr	MW	1360	8.7	0.054	0.065	0.084	0.12	11.1
NGC185		dSph	M31	175	8.6	0.0053	0.0053	0.090	0.51	10.5
NGC147		dSph	M31	101	8.4	0.032	0.036	0.050	0.17	12.4
IC1613		dIrr	M31	505	8.3	0.059	0.11	0.42	0.64	7.7
WLM	DDO221	dIrr	M31	840	8.2	0.14	0.35	0.55	0.69	6.7
Sex B	DDO70	dIrr	MW	1320	8.2	0.049	0.067	0.11	0.21	11.1
Sex A	DDO75	dIrr	MW	1440	7.9	0.15	0.29	0.38	0.41	9.3
Sagittarius		dSph	MW	28	7.7	0.0008	0.0008	0.52	0.86	6.5
Fornax		dSph	MW	138	7.5	0.013	0.059	0.33	0.73	7.4
UGC4879	VV124	dIrr	MW	1100	7.3					
Pegasus	DDO216	dIrr	M31	410	7.2	0.057	0.095	0.40	0.64	7.4
UGCA92	EGB_0427+63	dIrr	MW	1300	7.2					
Sag DIG	ESO594-4	dIrr	MW	1060	7.1	0.11	0.17	0.20	0.20	11.6
AndVII	Cassiopia dSph	dSph	M31	216	7.1	0.016	0.022	0.022	0.025	12.9
AndI		dSph	M31	48	7.1	0.0038	0.0098	0.087	0.67	8.9
AndII		dSph	M31	160	7.0	0.0049	0.0086	0.076	0.50	9.2
AndVI	Pegasus dSph	dSph	M31	266	6.9	0.0023	0.023	0.19	0.60	9.0
Leo A	DDO69	dIrr	MW	800	6.8	0.13	0.31	0.65	0.78	6.2
Antlia		dSph	MW	1330	6.8	0.043			0.43	9.0
LeoI	DDO74	dSph	MW	270	6.8	0.0099	0.18	0.50	0.76	6.4
Aquarius	DDO210	dIrr	MW	950	6.7	0.037	0.083	0.12	0.12	12.0
AndIII		dSph	M31	68	6.5	0.0022	0.0061	0.10	0.47	9.8
Cetus		dSph	M31	680	6.4	0.0045	0.013	0.17	0.52	9.9
LGS3	Pisces	dIrr	M31	284	6.3	0.015	0.046	0.16	0.43	9.8
LeoII	DDO93	dSph	MW	205	6.3	0.0028	0.012	0.025	0.70	8.8
Phoenix		dIrr	MW	405	6.3	0.027	0.071	0.23	0.42	10.3
Sculptor		dSph	MW	88	6.3	0.010	0.016	0.026	0.14	12.6
Tucana		dSph	MW	870	6.2	0.0048	0.011	0.014	0.30	11.6
AndXV		dSph	M31	170	6.2					
AndXVI		dSph	M31	270	6.1					
Sextans		dSph	MW	86	6.1	0.00	0.00	0.00	0.00	12.0
AndV		dSph	M31	117	6.0	0.0045	0.048	0.066	0.35	10.8
Carina		dSph	MW	94	6.0	0.0065	0.0077	0.43	0.67	7.1
Draco	DDO208	dSph	MW	79	5.9	0.0004	0.010	0.025	0.49	10.9
Ursa Minor	DDO199	dSph	MW	69	5.9	0.00	0.00	0.00	0.00	12.0
AndX		dSph	M31	110	5.9					
AndXIV		dSph	M31	162	5.8					
AndXVII		dSph	M31	44	5.8					
AndIX		dSph	M31	45	5.7					

Notes.—Listed are all presently known satellite galaxies of the MW and M31 within 1 h^{-1} Mpc of either host, with stellar mass $M_* > 5 \times 10^5\,{\rm M}_\odot$. Star formation data are shown if available – here we parameterize the SFH in terms of the fraction of total stellar mass formed in the last 1, 2, 5, and 10 Gyr (i.e., f_{1G}, f_{2G}, f_{5G}, f_{10G}) and the mean mass-weighted stellar age, τ. Most of the star formation data are derived from the Local Group Stellar Photometry Archive (Holtzman et al. 2006). Exceptions are M32, M33, Antlia, Sextans and Ursa Minor, which are taken from Dolphin et al. (2005) and τ is estimated from the reported f_{10G} value. The LMC data are inferred from Smecker-Hane et al. (2002); SMC from Harris & Zaritsky (2004). Distances from the host, $r_{\rm host}$, are directly taken or inferred from Grebel et al. (2003) with some exceptions: AndX (Zucker et al. 2007), AndXIV (Majewski et al. 2007), AndXV and AndXVI (Ibata et al. 2007), AndXVII (Irwin et al. 2008), UGC4879 (Kopylov et al. 2008), UGCA 92 (Mateo 1998), and M33 (McConnachie et al. 2004). Stellar mass, M_*, is from Dekel & Woo (2003), except for M32 and Sagittarius, whose values are estimated using $M_*/L_V = 3\ {\rm M}_\odot/{\rm L}_\odot$, with L_V from Mateo (1998); similarly we estimate M_* for AndIX, AndX, AndXIV, AndXV, AndXVI, AndXVII and UGC 4879 from the quoted L_V or M_V in the same references cited for $r_{\rm host}$.

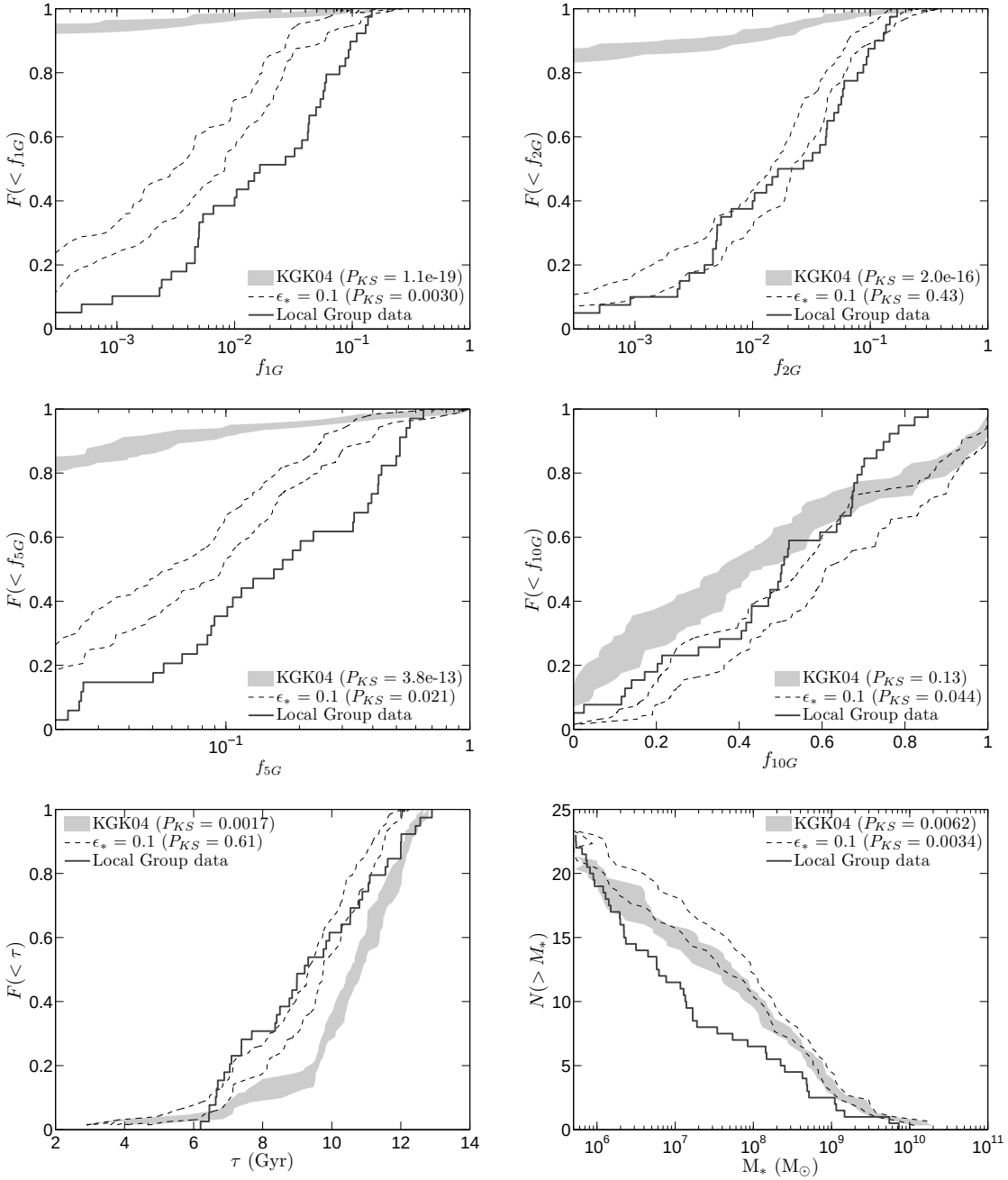

FIG. 1.— *Top four panels:* Cumulative distributions of the fractions of stellar mass formed in the last 1, 2, 5, and 10 Gyr. The f_{1G} and f_{2G} fractions reflect recent star formation, while the f_{5G} and f_{10G} fractions represent the overall star formation history. Solid line shows the data for the Local Group. Gray shaded region shows the spread of predictions of the KGK04 model, for 10 random realizations of the model. Dashed region shows the range predicted by our model with a stochastic star formation threshold, $\epsilon_* = 0.1$, also for 10 realizations. The numbers in parentheses show the Kolmogorov-Smirnov probability of the model average being consistent with the data. *Bottom left:* cumulative distribution of the mass-weighted mean age of stellar population. *Bottom right:* Cumulative stellar mass function per host halo.

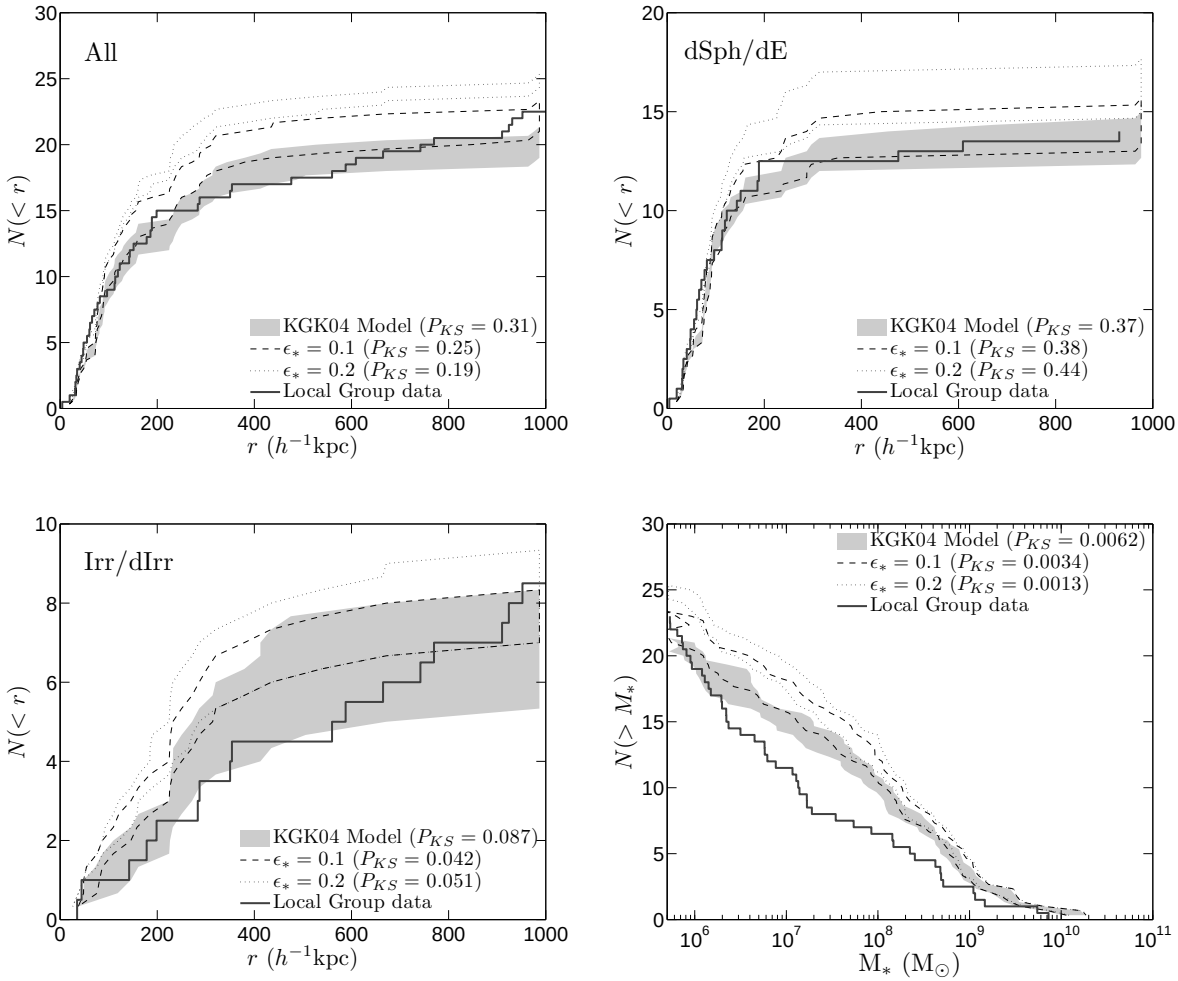

FIG. 2.— Three cumulative radial plots and a cumulative stellar mass function comparing the data for observed Local Group dwarfs (solid line) to three variants of the star formation model. The KGK04 model (gray shaded region) does not include stochasticity in the star formation density threshold, $\Sigma_{\rm th}$, (i.e., $\epsilon_* = 0$) whereas the two other models include stochasticity with a logarithmic dispersion $\epsilon_* = 0.1$ (contours of dotted lines) and $\epsilon_* = 0.2$ (contours of dashed lines). The other parameters of the Kennicutt-Schmidt law are kept the same for the three models. The models include an intrinsic spread from the random assignment of the angular momentum spin parameters to the halos. This spread is shown here as a filled region, or contours outlining a region, which encompasses the range of model predictions for 10 random realizations of the model.

TABLE 2
STOCHASTIC THRESHOLD OF STAR FORMATION LAW

	$\epsilon_* = 0$	$\epsilon_* = 0.05$	$\epsilon_* = 0.1$	$\epsilon_* = 0.15$	$\epsilon_* = 0.2$
P_{KS}: $r_{\rm all}$	3.1e-1	3.0e-1	2.5e-1	2.1e-1	2.2e-1
P_{KS}: $r_{\rm dSph}$	3.7e-1	3.6e-1	3.8e-1	3.6e-1	4.9e-1
P_{KS}: $r_{\rm dIrr}$	8.7e-2	5.2e-2	4.2e-2	3.3e-2	3.9e-2
P_{KS}: f_{1G}	1.1e-19	2.0e-6	3.0e-3	3.1e-2	1.1e-1
P_{KS}: f_{2G}	2.0e-16	3.4e-2	4.3e-1	3.6e-1	1.0e-1
P_{KS}: f_{5G}	3.8e-13	2.5e-4	2.1e-2	7.8e-2	2.9e-1
P_{KS}: f_{10G}	1.3e-1	9.9e-2	4.4e-2	1.6e-2	2.5e-3
P_{KS}: τ	1.7e-3	1.3e-1	6.1e-1	3.8e-1	1.5e-1
P_{KS}: M_*	6.2e-3	3.1e-3	3.4e-3	2.8e-3	1.2e-3
Dwarfs per halo	20	21	22	24	26

NOTES.—Other fixed parameters are $\Sigma_{\rm th0} = 5\ {\rm M}_\odot\ {\rm pc}^{-2}$, $f_{\rm sfr} = 1$. The observed number in the Local Group is $46/2 = 23$ dwarfs per host halo.

The last factor accounts for the less efficient gas dissipation in small halos with the virial temperature $T_{\rm vir} \lesssim$ few $\times 10^4$ K, or equivalently, maximum circular velocity $V_{\rm max} \lesssim 50$ km s^{-1}. This factor is written in terms of $V_4 \equiv 16.7\,{\rm km\,s^{-1}}$, the virial velocity corresponding to the virial temperature $T_{\rm vir} = 10^4$ K, and a constant, $c = 10$, chosen to reproduce the correct total number of dwarfs. This important factor, coupled with the density threshold for star formation, suppresses star formation in most low-mass halos. Equation (2) is consistent with results of recent hydrodynamic simulations of galaxy formation (Kravtsov & Gnedin 2005; Tassis et al. 2008). An alternative parametrization of dwarf gaseous disks with a temperature floor at $\sim 10^4$ K is given by Kaufmann et al. (2007). In their model the disks are vertically puffed-up, which works to the same effect to reduce the gas density. The observed stellar core radii in the Local Group dwarfs are a factor of $2-3$ smaller than those predicted by our model, which may favor the vertical expansion over the radial one assumed here. However, since it would not change the surface density Σ_g, we cannot fit it in our framework of the Kennicutt-Schmidt law of star formation.

The spin parameter λ is drawn randomly from a standard log-normal distribution with $\bar{\lambda} = 0.045$ and $\sigma_\lambda = 0.56$ (Vitvitska et al. 2002; Hernandez et al. 2007). This adds an intrinsic variance in the predictions of the star formation model. While the KGK04 model used only one set of the randomly-selected λ values to compare with the observations, in this paper we take 10 random realizations of each model, in order to account for this intrinsic variance.

The gaseous disk is modeled spatially by 50 radial zones. At each simulation output epoch (about every 10^8 yr), the newly accreted gas is added to these radial zones, according to the exponential profile of eq. (1). In each zone, the rate of star formation is determined by the Kennicutt-Schmidt law:

$$\dot{\Sigma}_* = 2.5\times 10^{-4} f_{\rm sfr} \left(\frac{\Sigma_g}{1\,{\rm M_\odot\,pc^{-2}}}\right)^n \,{\rm M_\odot\,kpc^{-2}\,yr^{-1}}, \quad (3)$$

wherever the gas density, Σ_g, exceeds the threshold, $\Sigma_{\rm th}$ (Kennicutt 1998). Standard parameters are $n \approx 1.4$, $f_{\rm sfr} = 1$, and $\Sigma_{\rm th} = 5\ {\rm M_\odot\,pc^{-2}}$. Most of the variants of the model discussed in this paper employ this star formation law but with an important addition, described in §4 below.

In addition to this quiescent mode of star formation, the model also allows a starburst mode prompted by strong tidal interactions with other halos (see section 6.1 in KGK04). In this mode there is no density threshold and even galaxies with $\Sigma_g < \Sigma_{\rm th}$ can form stars if a strong enough interaction occurs.

Finally, the effect of stellar evolution is taken into account following Prieto & Gnedin (2006). They find that some 40% of the initial stellar mass is lost to stellar wind and supernovae after $5-10$ Gyr, given the assumptions of the initial stellar mass function from Kroupa (2001), stellar remnant masses as a function of initial stellar mass from Chernoff & Weinberg (1990), and main sequence lifetimes from Hurley et al. (2000). In the models investigated here we simply assume that 40% of the initial stellar mass is lost between the time when the stars formed and the present day. We do not "recycle" the liberated gas back into the ISM, which would make it available to form more stars. As a result our estimate of the stellar masses are the lower limit of the true masses – a simple decrease of the total stellar mass, M_*, for each dwarf by a factor of 0.6. Accordingly, the $f_{[1,2,5,10]G}$ and τ values are unchanged by stellar evolution in our models and since the *HST* photometry for the Milky Way satellites is typically good enough to measure the main sequence stars we simply compare the observed $f_{[1,2,5,10]G}$ and τ values (Table 1) to the same quantities for the simulated dwarfs without any corrections.

We mark as luminous (having corrected M_* for stellar evolution as just described) those satellite halos with a predicted stellar mass $M_* > 5\times 10^5\,{\rm M_\odot}$ at $z = 0$. Such a cutoff agrees with the observational limit of all Local Group dwarfs (Table 1) known until a few years ago, when the ultrafaint dwarfs were discovered. We defer the discussion of the model predictions for these low-mass objects until §6.

As in KGK04, we do a rough morphological classification of dwarf galaxies as dSph or dIrr based on the ratio of the stellar rotation velocity to the velocity dispersion: $v_{\rm rot}/\sigma < 3$ for dSph and $v_{\rm rot}/\sigma > 3$ for dIrr. In the model, the rotation velocity is calculated as the circular velocity at the outer-most stellar radius, as it would be measured in observation, while the velocity dispersion is estimated from the amount of external tidal heating in strong tidal interactions with other halos. Such classification does not take into account the recent star formation activity or the remaining gas content, and therefore, is only a crude indication of the observationally defined morphological type. Comparison of these model predictions to the data is, in fact, completely complementary to the comparison of the star formation histories.

In the process of revising our models we have discovered that the gas densities Σ_g in Kravtsov et al. (2004) were underestimated by a factor of 2 due to an error in the code. When we quote the results for the KGK04 model here, we use the corrected values.

3.1. *Discrepancies of KGK04 Model with Star Formation Data*

Despite significant successes in explaining the number and spatial distribution of the Local Group dwarfs, the KGK04 model did not predict a sufficient amount of recent star formation. Figure 1 shows that 95% of the dwarfs in that model have not formed any stars in the last 1 Gyr, in serious disagreement with data.

To quantify the level of this disagreement, we use the Kolmogorov-Smirnov (KS) test for cumulative distribution functions of the following parameters: the distance to the host ($r_{\rm all}$), the distances for the dSph and dIrr galaxies separately ($r_{\rm dSph}$ and $r_{\rm dIrr}$), the star formation fractions (f_{1G}, f_{2G}, f_{5G}, f_{10G}), the mean age (τ), and the stellar mass (M_*). Table 2 shows that the recent star formation fractions in the KGK04 model (see column $\epsilon_* = 0$) have very low KS probabilities, below 10^{-12}. On the other hand, the f_{10G} fraction, which is a more global measure of the overall star formation, is consistent with the data at the 13% level. Thus the star formation law used in the model is not necessarily at fault, but the apparent lack of recent star formation is a direct result of the fixed star formation threshold, as we will see below.

The mean mass-weighted age is also inconsistent with the data, but at a less significant level ($P_{KS} \sim 10^{-3}$). The mean age is a global, integral measure of the SFH, which combines the low-probability recent star formation with a higher-probability early star formation. The stellar age is systematically overestimated in the model, by a few Gyr.

The total stellar mass is also overestimated by a factor of several for most dwarfs. The cumulative mass function is inconsistent with the data at a level similar to the age distribution, $P_{KS} \sim 10^{-3}$.

Note also that KGK04 considered principally the satellite dwarfs located within the virial radius of the host galaxy at $r < 200\,h^{-1}$ kpc. We extend our analysis to all dwarfs in the Local Group, even the potentially isolated ones lying outside the virial radius of either host. Figure 2 shows their cumulative radial distribution out to $1000\,h^{-1}$ kpc. The KGK04 model does well for the distribution of all dwarfs and the distribution of Irr/dIrr types separately. The model slightly overestimates the number of dSph/dE types outside $200\,h^{-1}$ kpc, but in all cases the KS probability is $\sim 10\%$ or higher, fully consistent with the observations.

Our phenomenological model contains several parameters that allow for some freedom in the outcome. Two of the most important parameters in the model are the threshold density $\Sigma_{\rm th}$ and the disk size parameter, c (eq. 2), both of which are difficult to know, *a priori*, from theory. Since these parameters can significantly change the predicted total number of dwarfs, the observed number of ($M_* > 5 \times 10^5 M_\odot$) dwarfs provides a fairly stringent constraint on these values. For example, with $c = 10$ and $\Sigma_{\rm th} = 5$ M$_\odot$ pc^{-2}, the predicted average number of dwarfs per host halo within 1 h^{-1} Mpc is 20.5. If we take $c = 5$ (with $\Sigma_{\rm th} = 5$ M$_\odot$ pc^{-2}) this number increases to 40.7, and if we take $c = 15$ the number of dwarfs drops to 14.3. Analogously, reducing the threshold density to 4 and 3 M$_\odot$ pc^{-2} (with $c = 10$) increases the average number to 21.7 and 22.3, respectively. None of these fixed threshold models, however, adequately reproduces the observed star formation histories. Therefore, we look for additional physical ingredients for our model.

In our extension of the KGK04 model, we attempt to retain the correct radial distribution of the dwarf galaxies, while improving the predictions for their star formation histories.

4. STOCHASTIC STAR FORMATION THRESHOLD

We consider a number of modifications to the KGK04 model. The most promising of the modifications is the introduction of a stochastic threshold to the star formation law.

At each output epoch through the course of the simulation, the threshold density for star formation is drawn from a log-normal distribution with a mean value $\Sigma_{\rm th0}$ and a small dispersion $\epsilon_* \sim 0.1$:

$$P(\Sigma_{\rm th})\,d\Sigma_{\rm th} = \frac{1}{\sqrt{2\pi}\epsilon_*} \exp\left[-\frac{(\log\Sigma_{\rm th} - \log\Sigma_{\rm th0})^2}{2\epsilon_*^2}\right] d\Sigma_{\rm th}. \quad (4)$$

As a fiducial mean value we take $\Sigma_{\rm th0} = 5$ M$_\odot$ pc^{-2}, but we also vary that parameter in some runs.

What does this stochastic threshold mean? And what, physically, is the threshold of star formation? We apply it to the azimuthally-averaged surface density of gas. In nearby star forming regions, which we can study directly with *HST* and *Spitzer*, stars form in dense molecular clouds (e.g., McKee & Ostriker 2007). Locally the density is high, but the azimuthal average at a particular distance r from the center may be either high (if molecular clouds are common at r) or low (if they are rare). Thus, by invoking the threshold $\Sigma_{\rm th}$, we are effectively parameterizing the fraction of molecular gas available for star formation. When we take the threshold to vary, we are thus accounting for stochastic star formation in isolated HII regions, such as those found by *GALEX* in nearby spirals (Thilker et al. 2007).

Nearby dwarf galaxies often show a very high HI gas fraction, i.e. the ratio of gas mass to baryon (gas+stars) mass, up to 90% (Fisher & Tully 1975; Geha et al. 2006; Lee et al. 2006). The current star formation rates in those galaxies are low, and therefore most of the gas is inert. Hydrodynamic simulations of Robertson & Kravtsov (2008), which treat the formation of molecular hydrogen in detail, also suggest that dwarf disks may contain large reservoirs of diffuse atomic gas that is unable to condense in molecular clouds and participate in star formation. This inefficiency of forming molecular clouds at low densities effectively results in the threshold density for star formation.

4.1. *A Major Improvement*

Figure 1 shows that the stochasticity greatly improves the agreement of the recent star formation fractions ($f_{1G}, f_{2G},\ f_{5G}$) with the Local Group data. The predicted distributions are much closer to the observed ones than in the KGK04 model, and are, in fact, statistically consistent with each other at $\sim 10\%$ level.

We quantify this effect by gradually increasing the amount of stochasticity, ϵ_*. Table 2 shows the KS test results for ϵ_* ranging from 0.05 to 0.2, which approximately corresponds to 10% to 60% variation in the threshold density $\Sigma_{\rm th}$. Even a small amount of stochasticity, $\epsilon_* \sim 0.05$, leads to a dramatic improvement of the f_{1G}, f_{2G}, and f_{5G} statistics. The probabilities increase rapidly with ϵ_* to a good fraction of a percent or more. The model with $\epsilon_* = 0.1$ is already statistically consistent with the data.

With the other parameters of the star formation law ($\Sigma_{\rm th0}$ and $f_{\rm sfr}$) being fixed, increasing ϵ_* leads to better recent star formation parameters but worse early star formation parameters. The probability of the f_{10G} distribution decreases from 13% to under 5% for $\epsilon_* = 0.1$ and even below a percent for $\epsilon_* = 0.2$.

The mean age is most consistent with the data ($P_{KS} = 0.61$) for $\epsilon_* = 0.1$. The total number of dwarfs also increases systematically with ϵ_* while the stellar mass function and the radial distributions are not significantly affected by the variation of ϵ_*. Additionally, the $\epsilon_* = 0.15$ and $\epsilon_* = 0.2$ models begin to overpredict the total number of luminous dwarfs per host halo, implying that at these values the overall star formation becomes too efficient. This overabundance can be seen in Table 2, or graphically in Fig. 2. Therefore, we take the case with $\epsilon_* = 0.1$ as our fiducial model striking the best balance for all star formation statistics. We consider other variants of the stochastic model in §5.

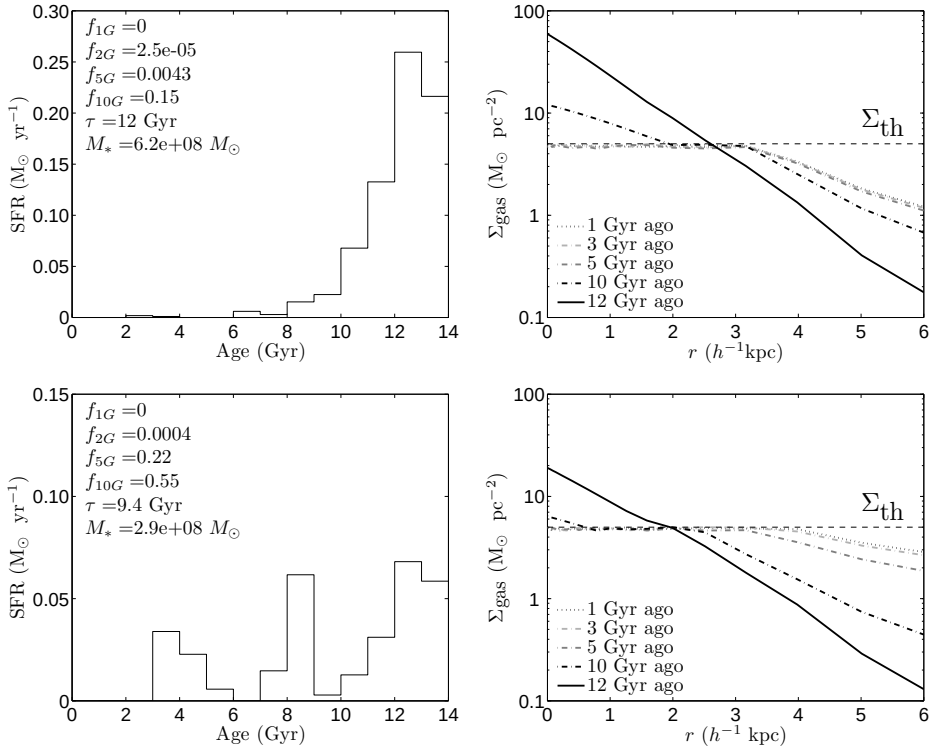

FIG. 3.— *Left:* The star formation histories of two simulated dwarfs in the KGK04 model, coarsened into 1 Gyr bins so as to better resemble the time resolution of the data. The x-axis shows the Age (i.e. of the isochrone) with the present epoch at 0 Gyr, going back to the Big Bang at 14 Gyr. *Right:* The gas density profiles for the two simulated galaxies that were used to calculate their star formation rates, at five epochs. The fixed star formation threshold is shown by the dashed horizontal line.

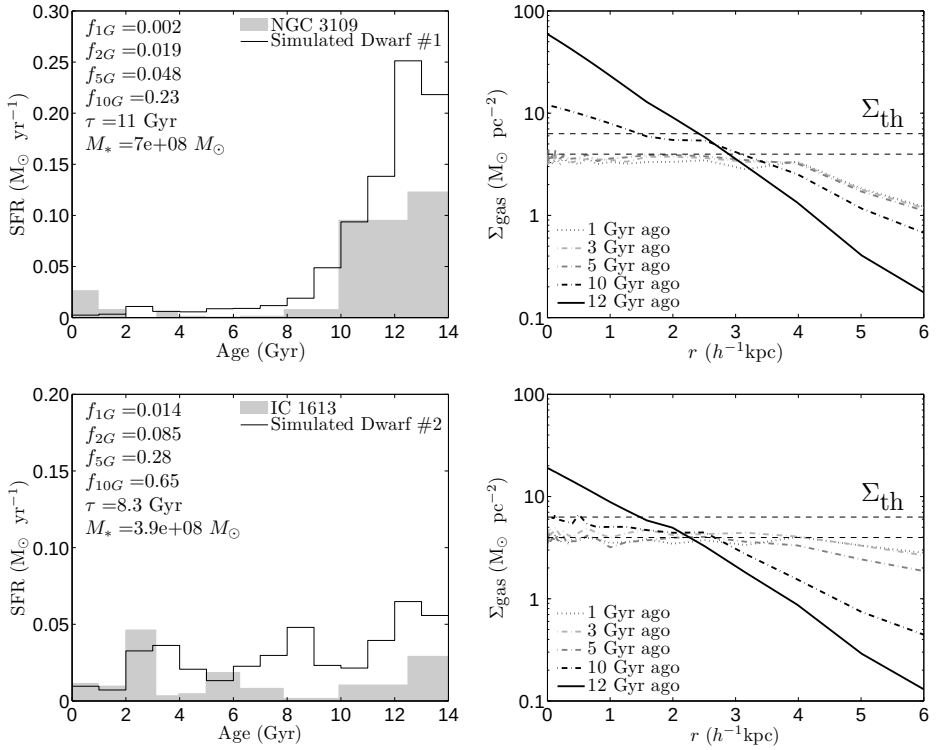

FIG. 4.— *Left:* The star formation histories of the two dwarfs from Fig. 3 in the model with a stochastic star formation threshold, $\epsilon_* = 0.1$ (dashed histograms and quoted parameters). For comparison, shaded histograms show the observed SFHs of NGC 3109 and IC 1613, normalized to the total stellar mass cited in Table 1. *Right:* The gas density profiles at five epochs. The range of variation of the star formation threshold is shown by dashed horizontal lines. This range allows star formation to continue at late times.

4.2. *Reasons for Success*

Figures 3 and 4 illustrate why the stochasticity is so successful. They show star formation histories and corresponding gas density profiles for two representative model dwarfs. Figure 3 is for the case of a fixed density threshold, $\Sigma_{\rm th} = 5$ M$_\odot$ pc^{-2}. Without the stochasticity, and in the absence of radial gas flows, the gas above the threshold is steadily converted into stars at early times (10 and 12 Gyr ago) at substantial rates, $0.1 - 0.3$ M$_\odot$ yr^{-1}. At these epochs the galaxies evolve effectively in isolation, while still growing by gas-rich hierarchical mergers. At later time, when these galaxies become satellites of the larger host galaxy, they are tidally truncated and no new gas is accreted. After the high-density gas supply is exhausted, the rest of the gas hovers just under the threshold, unable to form new stars. In the first dwarf, shown in the top panels in Figure 3, star formation almost completely halts 8 Gyr ago. The other dwarf, shown in the bottom panels, experiences several distinct episodes of star formation, the last one finishing 3 Gyr ago. In both cases there is effectively no star formation in the last 2 Gyr, $f_{1G} \approx f_{2G} \approx 0$.

If instead the threshold density varies in time, at later epochs the gas may find itself above the threshold and allow more recent star formation. Figure 4 shows the star formation histories for the same dwarfs but now with a variable threshold and using $\epsilon_* = 0.1$. There is more star formation overall and more star formation at later times. As a result, the stellar mass is higher by 20% to 30% and mean stellar age is lower by about 1 Gyr. More importantly, several percent of all stars are formed in the last 2 Gyr. This stochastic enhancement of the star formation rate allows the model to reproduce the star formation episodes at late times when gas-rich mergers (which increase the available gas supply) and strong interactions (which can prompt starbursts) are relatively less common.

We also show on Fig. 4 the observed star formation histories of two dwarf galaxies, NGC 3109 and IC 1613. We do not expect the model predictions to correspond in detail to the observed SFH features, as our modeling is necessarily statistical and is aimed at explaining not a specific galaxy's SFH but only an ensemble of SFHs of many Local Group dwarfs. Still, qualitatively, the agreement between the model and the data is good: in the case of NGC 3109 both show most stars being formed at early times with a small fraction in the last 4 Gyr, while in the case of IC 1613, both SFHs continue until the present in several distinct, extended episodes.

4.3. *Remaining Discrepancies*

Despite the impressive improvements, there still remain discrepancies of the fiducial model with the observed data.

First, there is still not quite enough very recent star formation, a problem which is quantified by the KS-test result for f_{1G} in Table 2 ($P_{KS} \approx 3 \times 10^{-3}$) and is apparent in Fig. 1. The models with a higher amount of stochasticity, $\epsilon_* = 0.15$ and $\epsilon_* = 0.2$, achieve better agreement with the observed f_{1G} distribution but they are disfavored for skewing all other star formation statistics. Thus, in the fiducial model ($\epsilon_* = 0.1$) over 25% of the dwarfs have less than 10^{-3} of their stars formed in the last 1 Gyr, compared with about 10% of such dwarfs in the observed sample. Note that the current observations are sensitive to SFHs with large fractions of star formation at later times. The very deep *HST* ACS imaging of Leo A by Cole et al. (2007) have confirmed that majority of all star formation has occurred in the last half of the age of the universe.

TABLE 3
Gas Accretion at $d < R_{\rm vir}$

	No	Yes
P_{KS}: $r_{\rm all}$	2.5e-1	2.4e-1
P_{KS}: $r_{\rm dSph}$	3.8e-1	4.1e-1
P_{KS}: $r_{\rm dIrr}$	4.2e-2	3.1e-2
P_{KS}: f_{1G}	3.0e-3	9.1e-2
P_{KS}: f_{2G}	4.3e-1	8.1e-1
P_{KS}: f_{5G}	2.1e-2	1.9e-1
P_{KS}: f_{10G}	4.4e-2	5.8e-3
P_{KS}: τ	6.1e-1	3.8e-1
P_{KS}: M_*	3.4e-3	6.3e-4
Dwarfs per halo	22	23

Note.—Other parameters are $\epsilon_* = 0.1$, $\Sigma_{\rm th0} = 5$ M$_\odot$ pc^{-2}, $f_{\rm sfr} = 1$.

Second, the total stellar masses of the luminous dwarfs in the models tend to be significantly above the observed stellar masses of the Local Group dwarfs. This result is apparent for any value of ϵ_* between 0 and 0.2 (see bottom right panel of Fig. 2). This excess stellar mass in our models can perhaps be traced to the fact that we do not include thermal and ionizing feedback from young massive stars (e.g., Dekel & Silk 1986; Dekel & Woo 2003), which can disrupt molecular clouds and drive galactic outflows, thus reducing the available gas supply for star formation.

Third, the model does not predict enough very *early* star formation. This is a generic problem with any hierarchical model in which the presently-massive satellites form and accrete onto the host late and, at early times, therefore, do not contain significant amounts of gas above the threshold. Our model predicts that some 20% to 30% of the dwarf galaxies will have formed greater than 85% of their stellar mass in the last 10 Gyr (i.e. $f_{10G} > 0.85$). In other words, there exists in the model a number of dwarfs with anomalously young stellar populations, whereas, by contrast, the Local Group data in Table 1 does not show any dwarfs having formed more than 86% of its stellar mass in the last 10 Gyr (the Saggitarius dSph has the highest fraction) – at least 14% of all stars in the observed dwarfs formed in the first 4 Gyr after the Big Bang. Some of the simulated dwarfs with very young stellar populations include objects which form the bulk of their stars in one, punctuated star formation event caused by a close tidal interaction, prompting a starburst which happened to occur in the last 10 Gyr. But not all of the galaxies in this category form stars through the starburst mode; other dwarfs with very young stellar populations form all of their stars through the continuous mode with no starbursts at all.

5. OTHER VARIANTS OF STAR FORMATION MODEL

With the discrepancies discussed in §4.3 in mind, we have explored several variants of our star formation

model in order to check if relaxing other model assumptions can improve the predicted star formation histories to the point where there is broad agreement with the observations.

5.1. *Gas Accretion within the Virial Radius*

One of these alternate models is motivated by the lack of enough recent star formation. In the KGK04 model and in the stochastic models shown in Figs. 1 and 2, accretion of new gas onto the dwarf halos is shut off whenever the dwarf comes within the virial radius of the host halo. This is based on the expectation that satellite halos near their host would be tidally truncated and unable to capture new gas even if they happen to increase their dark matter mass in mergers with other satellite halos. However, becoming a satellite does not immediately stop the halo's star formation activity which can continue as long as the gas density remains above the threshold or if a starburst event is triggered.

In the first of these alternative models, we lift this assumption and allow the accretion of new gas even within the virial radius of the host, at $d < R_{\rm vir}$. As a result, the agreement between the model and the data for the f_{1G} distribution improves as indicated by the KS-test results shown in Table 3 – from the rejection of the null hypothesis of the same-distribution at 0.3% significance level to rejection only at the 9% level, essentially statistically consistent.

Qualitatively, the improvement is most dramatic for f_{1G} since allowing the additional accretion of gas is more important at late times, and because the virial radius of the host halo will be larger than at earlier epochs; also the dwarf galaxies at late times are likely to be closer in. The extra gas is converted into extra stars and so the f_{1G} value increases and the typical mass of the dwarfs increases. Generally, the extra accretion shifts the stellar age distribution to be younger. However, another predicted feature of our models is a tail of the age distribution at $\tau < 5$ Gyr. The extra accretion exaggerates this tail since it increases recent star formation. In contrast, the youngest dwarf galaxy in the Local Group is Leo A, with $\tau = 6.2$ Gyr (though see the Leo A SFH of Cole et al. 2007, which has a significantly younger result for τ). This is fundamentally the same problem as the existence of simulated dwarfs with $f_{10G} > 0.85$, and the f_{10G} distribution similarly becomes less consistent with the data in this model.

5.2. *Modifications of the Schmidt Law*

Another important question to be addressed is whether the observed SFHs, given our model assumptions, favor steepening of the Schmidt-Kennicutt law ($\dot{\Sigma}_* \propto \Sigma_g^n$). There is some evidence for the exponents n to become gradually larger at low gas densities in dwarf galaxies (e.g., Boissier et al. 2003; Heyer et al. 2004; see also discussion in Robertson & Kravtsov 2008). Since most of our dwarfs are close to the threshold, we investigate this effect simply by changing the exponent at all densities, setting it to $n = 1.4$, 2, or 3. For each of these values, the normalization $f_{\rm sfr}$ is allowed to float such that the overall star formation efficiency is lowered until the point where the median of the age distribution, $\tau_{\rm med}$, of the simulated dwarfs matches that of the Local Group galaxies, 9.25 Gyr.

TABLE 4
Slope of Schmidt law, $\dot{\Sigma}_* \propto \Sigma_g^n$

	$n = 1.4$	$n = 1.4$	$n = 2$	$n = 3$
$f_{\rm sfr}$	1	0.5	0.14	0.012
P_{KS}: $r_{\rm all}$	2.5e-1	2.5e-1	2.6e-1	2.6e-1
P_{KS}: $r_{\rm dSph}$	3.8e-1	4.4e-1	4.2e-1	4.8e-1
P_{KS}: $r_{\rm dIrr}$	4.2e-2	3.5e-2	3.3e-2	3.5e-2
P_{KS}: f_{1G}	3.0e-3	1.4e-2	2.5e-2	8.3e-2
P_{KS}: f_{2G}	4.3e-1	2.4e-1	2.4e-1	1.8e-1
P_{KS}: f_{5G}	2.1e-2	1.1e-1	9.4e-2	1.3e-1
P_{KS}: f_{10G}	4.4e-2	5.7e-3	7.7e-3	8.3e-3
P_{KS}: τ	6.1e-1	1.1e-1	4.5e-1	5.2e-1
P_{KS}: M_*	3.4e-3	3.7e-3	3.1e-3	5.0e-3
Dwarfs per halo	22	22	22	21

Note.—Other parameters are $\epsilon_* = 0.1$, $\Sigma_{\rm th0} = 5$ M$_\odot$ pc^{-2}.

Table 4 shows the required values of $f_{\rm sfr}$ and the results of KS-tests. The rather high significance results from the KS tests applied to the τ-distribution are not particularly surprising since the normalization of the star formation law has been fine-tuned for this comparison. Qualitatively this exercise keeps the overall star formation rate the same, i.e. the stellar mass function is basically unchanged. And similarly the radial distributions stay roughly the same – this is important since one of the primary successes of the KGK04 model was reproducing the observed radial distribution of the Local Group dwarfs, something that our models continue to do. Eventually the same amount of gas above the density threshold is converted into stars, so the rate at which star formation proceeds does not alter the total number or the radial distribution of the simulated dwarfs.

By and large, all of the same discrepancies with the data listed in §4.3 are apparent in these models with different n – too large stellar masses, not enough recent star formation, and too much overall star formation in the last 10 Gyr. Arguably the $\{n = 3,\ f_{\rm sfr} = 0.012\}$ model is a best fit to the data for f_{1G} and f_{5G}, however the fiducial $\{n = 1.4,\ f_{\rm sfr} = 1\}$ model is still the best for f_{2G} and f_{10G}. Further, comparisons of the stellar mass and the τ-distribution are inconclusive as well.

5.3. *Revised Epoch of Reionization and Cutoff Mass*

Another interesting test is to vary the epoch of reionization. Appendix B of KGK04 presents an analytic fit to the numerical results of Gnedin (2000) that parametrize the reionization epoch in terms of the redshift when cosmic HII regions begin to overlap, z_o, and the redshift when the reionization is completed, z_r. Varying these two parameters allows us to test the sensitivity of model predictions to the details of the evolution of the ionizing background radiation. Note that our parametrization of reionization here applies only to the local neighborhood of the Galaxy and may differ from the global cosmic reionization.

Reionization affects the amount of gas accreted onto dwarf halos. Increasing extragalactic UV flux during reionization photoionizes the gas inside and outside dark matter halos and prevents the halos with shallow potential wells from capturing new gas heated to $\sim 10^4$ K. In Gnedin (2000) the effect of decreasing the gas fraction of

TABLE 5
Reionization Scenarios

	Early	Extended	Fiducial	Late
z_r	9	7	7	6
z_o	10	10	8	10
P_{KS}: $r_{\rm all}$	2.3e-1	2.9e-1	2.5e-1	3.2e-1
P_{KS}: $r_{\rm dSph}$	5.7e-1	5.6e-1	3.8e-1	5.3e-1
P_{KS}: $r_{\rm dIrr}$	4.2e-2	4.7e-2	4.2e-2	6.0e-2
P_{KS}: f_{1G}	1.6e-2	7.7e-3	3.0e-3	1.3e-2
P_{KS}: f_{2G}	7.7e-1	6.4e-1	4.3e-1	6.6e-1
P_{KS}: f_{5G}	1.2e-1	8.2e-2	2.1e-2	6.3e-2
P_{KS}: f_{10G}	4.8e-3	9.9e-3	4.4e-2	1.5e-2
P_{KS}: τ	6.3e-1	6.9e-1	6.1e-1	6.7e-1
P_{KS}: M_*	1.6e-3	1.3e-3	3.4e-3	2.4e-3
Dwarfs per halo	20	19	22	18

Notes.—z_r refers to the redshift when reionization is completed, while z_o refers to the redshift where cosmic HII regions begin to overlap (see Appendix B in Kravtsov et al. 2004 for details). Other parameters: $\epsilon_* = 0.1$, $\Sigma_{\rm th0} = 5$ $\rm M_\odot\,pc^{-2}$, $f_{\rm sfr} = 1$.

halos was parametrized as

$$f_{\rm gas} = f_{\rm b}\,(1 + M_c/M)^{-3}, \quad (5)$$

where $f_{\rm b}$ is the universal baryon fraction, M is the halo mass, and M_c is the cut-off mass parameter. In linear theory for baryon perturbations, this parameter can be related to the filtering mass as $M_c \approx 0.26\,M_f$. The filtering mass M_f is an integral of a function of the intergalactic gas temperature over cosmic history and corresponds to the mass of a halo that loses 50% of its baryons as a result of external photoheating. The values of the filtering mass from Gnedin (2000) can be calculated for any z_o and z_r using eq. (B1) in Kravtsov et al. (2004).

We consider four scenarios listed in Table 5: early $\{z_r = 9,\ z_o = 10\}$, extended $\{z_r = 7,\ z_o = 10\}$, and late $\{z_r = 6,\ z_o = 10\}$ reionizations, in addition to the standard scenario $\{z_r = 7,\ z_o = 8\}$, which was used in KGK04 and in our fiducial model. Generally, the results are quite similar for all scenarios, likely because luminous satellites are hosted by the relatively massive halos, in which the virial temperatures are above 10^4 K and the external heating of the gas does not affect its distribution significantly. Early reionization is slightly preferred for the f_{1G}, f_{2G}, and f_{5G} distributions, but statistically all scenarios are consistent with each other. The f_{10G} distribution is still reproduced best by the fiducial model.

Recent hydrodynamic simulations indicate that the filtering mass may overestimate the mass of the halos that lose 50% of their baryons, especially at low redshift. The most sophisticated ART simulations of Tassis et al. (2008), including the effects of radiative transfer, give distributions of $f_{\rm gas}$ at several redshifts, $z = 3.3, 4, 5, 7, 8, 9$ (their Fig. 2) for the standard model of reionization. We have fit these distributions with the form of equation (5) and obtained best-fitting values of M_c. These values are similar to our old values at $z \geq 8$ but deviate from them at lower redshift by as much as an order of magnitude. We supplement these high-redshift fits with the $z = 0$ results of SPH simulations by Crain et al. (2007) and Hoeft et al. (2007), which both give $M_c \sim 2 \times 10^9\,h^{-1}$ $\rm M_\odot$, about a factor of 5 smaller than our old value. The combined sets at $z = 0$ and $z > 3$ can be fit by the following expression, accurate to better than 50%:

$$M_c \approx 1.8 \times 10^7 + 3 \times 10^9\,(1+z)^{-3}\ h^{-1}\,\rm M_\odot. \quad (6)$$

Ideally, we would like to derive the cutoff mass evolution from several simulations covering the whole range of redshifts, but at the moment it is the best we can assemble from the literature.

We have run our model with the new expression (6) for M_c and found that the corresponding changes in the predicted SFHs are not straightforwardly better or worse. The f_{1G} distribution improves a little, f_{2G} and f_{5G} are effectively unchanged, while the f_{10G} distribution is significantly worse off and the anomalously young dwarfs still persist. The age distribution and stellar mass function are also more discrepant with the data than in the fiducial model. While the lack of improvement with the new cutoff mass prescription is unpleasant or, at any rate, suprising, until we have a more robust estimate of M_c confirmed by several groups, we keep our fiducial model untouched.

5.4. *Monotonically Variable Star Formation Threshold*

In addition to exploring the stochastically variable density threshold, we have also investigated a threshold $\Sigma_{\rm th}$ that varies with redshift monotonically. Though, at the moment, we do not know of a convincing physical motivation for such a global systematic variation, we have investigated this possibility in exploring the full range of predictions of our model. Here we used a simple parameterization of the $\Sigma_{\rm th}$ redshift dependence,

$$\Sigma_{\rm th}(z) = \Sigma_{\rm th0}\,(1+z)^{\alpha}, \quad (7)$$

where $\Sigma_{\rm th}(z = 0) = \Sigma_{\rm th0} = 3$ $\rm M_\odot\,pc^{-2}$ and $\Sigma_{\rm th}(z = 9) = 5$ $\rm M_\odot\,pc^{-2}$, which results in $\alpha = \log(5/3) \approx 0.22$.

Interestingly, the results of this model are very similar to our fiducial model with the stochastic threshold. The comparison is shown in Table 6. The new model shares the same problems as the fiducial model: the stellar masses are still too large and the anomalously young dwarf problem is still present (if not slightly worse). We do not consider any other variants of the monotonic threshold but note that if a compelling theoretical or observational motivation for such a variation appears in the future, an evolving threshold may become a viable model.

TABLE 6
Stochastic vs. Monotonic Threshold of Star Formation Law

	$\epsilon_* = 0$ $\Sigma_{\rm th0} = 5$	$\epsilon_* = 0.1$ $\Sigma_{\rm th0} = 5$	$\epsilon_* = 0$ $\Sigma_{\rm th}(z)$
P_{KS}: $r_{\rm all}$	3.1e-1	2.5e-1	3.0e-1
P_{KS}: $r_{\rm dSph}$	3.7e-1	3.8e-1	3.4e-1
P_{KS}: $r_{\rm dIrr}$	8.7e-2	4.2e-2	3.7e-2
P_{KS}: f_{1G}	1.1e-19	3.0e-3	3.7e-2
P_{KS}: f_{2G}	2.0e-16	4.3e-1	7.1e-1
P_{KS}: f_{5G}	3.8e-13	2.1e-2	1.6e-2
P_{KS}: f_{10G}	1.3e-1	4.4e-2	2.7e-2
P_{KS}: τ	1.7e-3	6.1e-1	5.0e-1
P_{KS}: M_*	6.2e-3	3.4e-3	2.0e-3
Dwarfs per halo	20	22	23

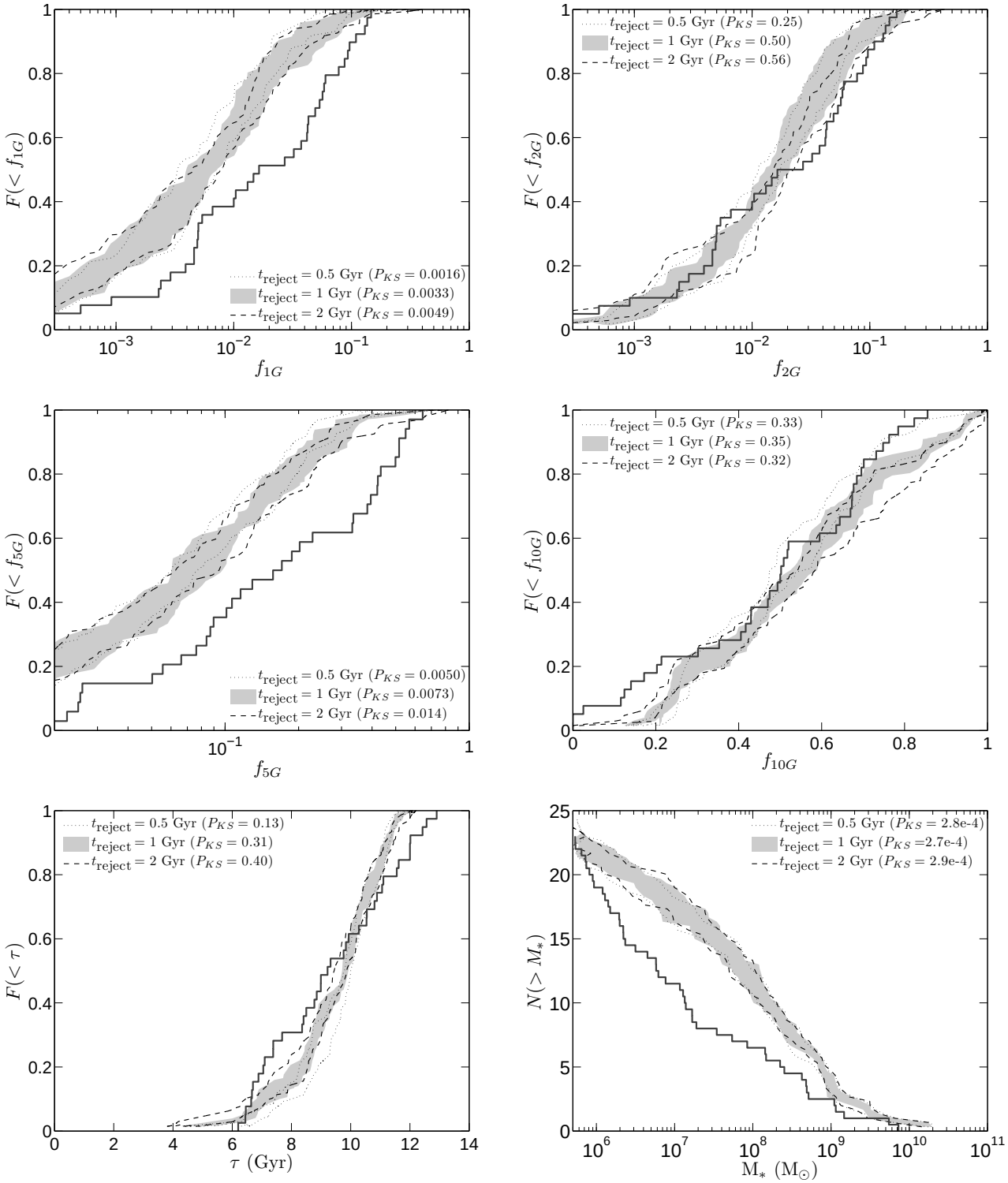

FIG. 5.— A comparison of three variants of the fiducial model which reject dwarfs that have not formed any stars by $t_{\rm reject} = 0.5$ Gyr (filled gray shape), $t_{\rm reject} = 1.0$ Gyr (dashed line), or $t_{\rm reject} = 2.0$ Gyr (dotted line) after the Big Bang. Local Group data are shown as a solid black line. Note that in order to match the observed number of dwarfs, the star formation density threshold is lowered in these models, see Table 7. The only noticeable improvements, relative to the fiducial model, are in the f_{10G} distribution and in the corresponding lack of the low-τ tail in the age distribution.

TABLE 7
Rejecting Late Beginners

	$t_{\rm reject}$ = 0.5 Gyr	$t_{\rm reject}$ = 1 Gyr	$t_{\rm reject}$ = 2 Gyr	No rejection
$\Sigma_{\rm th0}$	1.87	2.6	3.5	5.0
P_{KS}: $r_{\rm all}$	5.3e-1	4.0e-1	3.4e-1	2.5e-1
P_{KS}: $r_{\rm dSph}$	1.7e-1	3.7e-1	5.1e-1	3.8e-1
P_{KS}: $r_{\rm dIrr}$	2.2e-1	9.6e-2	7.3e-2	4.2e-2
P_{KS}: f_{1G}	1.6e-3	3.3e-3	4.9e-3	3.0e-3
P_{KS}: f_{2G}	2.5e-1	5.0e-1	5.6e-1	4.3e-1
P_{KS}: f_{5G}	5.0e-3	7.3e-3	1.4e-2	2.1e-2
P_{KS}: f_{10G}	3.3e-1	3.5e-1	3.2e-1	4.4e-2
P_{KS}: τ	1.3e-1	3.1e-1	4.0e-1	6.1e-1
P_{KS}: M_*	2.8e-4	2.7e-4	2.9e-4	3.4e-3
Dwarfs per halo	22	22	23	22

Notes.—Here we reject dwarfs that have not formed any stars by $t_{\rm reject}$ = 0.5 Gyr, 1 Gyr, or 2 Gyr after the Big Bang (redshifts $z \approx 10$, $z \approx 6$, and $z \approx 3.3$, respectively). Other parameters: $\epsilon_* = 0.1$, $f_{\rm sfr} = 1$.

5.5. *Rejecting Galaxies with Delayed Star Formation*

Finally, in directly addressing the problematic issue of the simulated dwarfs with too young stellar populations, we consider models that reject dwarfs with delayed star formation, i.e. the dwarfs that have not formed any stars within the first few Gyr after the Big Bang.

The reasoning for such an *ad hoc* cut is motivated by the uncertainty in the detailed effect of the early UV background on the gas content of low-mass halos. The satellites without early star formation in our model must have acquired a significant gas reservoir only at late times. In the hierarchical paradigm, these satellites have been built by mergers of smaller objects, each of which carried an even smaller amount of gas. In order to become a galaxy in our model, at some time the total gas density distribution in the satellite must reach above the density threshold. However, if for any reason we underestimated the effect of gas loss from small halos at early times, then at that time the combined amount of gas would be overestimated and star formation should not take place. Our treatment of the gas heating during reionization is very approximate, which makes it likely that we could either underestimate or overestimate the gas loss effect for particular dwarfs. In general, star formation at very high redshift could proceed even at lower densities than assumed in our models, such that all luminous dwarfs form at least a fraction of their stars before reionization (Ricotti & Gnedin 2005).

In the current concordance cosmology (Komatsu et al. 2008), the epoch of complete reionization can range from $z \sim 10$ to $z \sim 6$, which corresponds to a range of times from 0.5 to 1 Gyr after the Big Bang. Given this uncertainty, and uncertainties in the details of gas outflows, we consider three models that reject the dwarfs without star formation in the first 0.5 Gyr, 1 Gyr, or 2 Gyr after the Big Bang. The last model with $t_{\rm reject}$ = 2 Gyr is the least restrictive and closest to the fiducial model (no rejection), which can be formally written as $t_{\rm reject} > 14$ Gyr. In each of these "reject late beginners" models, the star formation density threshold $\Sigma_{\rm th0}$ is lowered in order to raise the number of dwarfs back to the number observed in the Local Group. The details of these models are listed in Table 7.

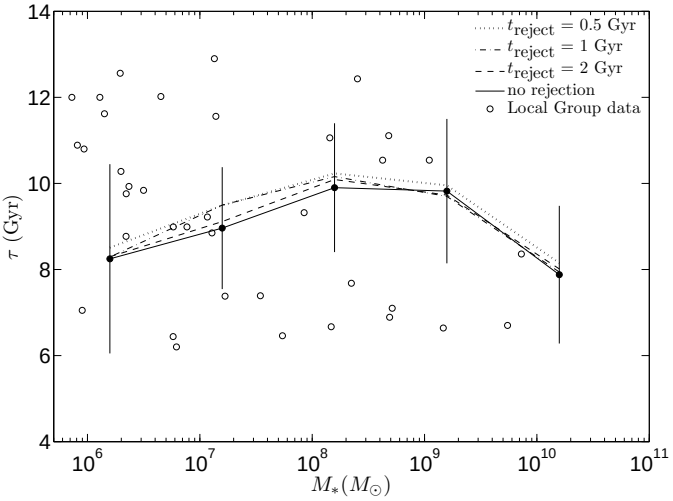

Fig. 6.— Mass-weighted mean stellar age vs. stellar mass at $z = 0$. We show the fiducial model and three variants, which reject simulated galaxies with delayed star formation, by 0.5, 1, and 2 Gyr, respectively. The model galaxies are binned by stellar mass and only the bin averages are shown for clarity. Vertical bars indicate the standard deviation of the sample in each bin. Observed values for the Local Group (Table 1) are plotted by circles and fall in the same range as the model.

Figure 5 shows the star formation parameters in the three models. All of the distributions are similar to each other, but they all deviate from the fiducial model (plotted in corresponding panels of Fig. 1) in one important aspect. The f_{10G}-distribution lacks objects with $f_{10G} = 1$, i.e. with no star formation in the first 4 Gyr after the Big Bang. Unfortunately, the time resolution of the observed SFHs does not allow us to discriminate among the three variants of the cut. But all of them provide the needed fix: the f_{10G}-distribution is fully consistent with the data ($P_{KS} > 30\%$).

Table 7 shows that the other probabilities remain roughly the same or even decrease relative to the fiducial model. If we are to accept any of the "reject late beginners" variants, we would prefer the least restrictive $t_{\rm reject}$ = 2 Gyr model. Ideally, of course, we prefer to develop a better understanding of early star formation that would make this cut unnecessary.

Figure 6 shows the stellar age as a function of stellar mass in the fiducial model and its three variants. Rejecting any of the "late beginners" increases the stellar age by less than 1 Gyr, which is significantly smaller than the dispersion of the sample at all masses. A general trend, also largely overcome by the dispersion, is for the mean age to increase with mass until $M_* \sim 10^9\,{\rm M}_\odot$ and then to decrease at larger masses. The Local Group data are consistent with the younger stellar ages, and extended SFHs, for more massive galaxies. At the lowest-mass end, however, the observations show a number of very old objects that are still not present in our models, even with the strictest age cut. It is apparent from this and previous plots that our prescription for star formation in the first few Gyr of cosmic time still needs improvement.

It is possible that the starburst mode of star formation is causing very young stellar ages in small galaxies. We have checked, however, that the anomalously young dwarfs do not all have significant starbursts at late times

TABLE 8
Low Mass Satellite Galaxies of MW and M31

Galaxy	Host	$r_{\rm host}$ (kpc)	M_V	M_* ($M_\odot$)	Refs
Leo T	MW	417	−8.0	4.0×10^5	1
Canes Venatici I	MW	218	−7.9	3.7×10^5	2
AndXI	M31	103	−7.3	2.1×10^5	3
AndXIII	M31	95	−6.9	1.5×10^5	3
AndXII	M31	116	−6.4	9.3×10^4	3
Hercules	MW	138	−6.0	6.4×10^4	4
BoötesI	MW	62	−5.8	5.4×10^4	5
Ursa Major I	MW	106	−5.6	4.5×10^4	6
LeoIV	MW	158	−5.1	2.8×10^4	4
Canes Venatici II	MW	151	−4.8	2.1×10^4	4
SDSSJ100+5730	MW	83	−4.2	1.2×10^4	7
SDSSJ1329+2841	MW	76	−3.9	9.4×10^3	7
Ursa Major II	MW	32	−3.8	8.5×10^3	8
Coma Berencies	MW	44	−3.7	7.8×10^3	4
BoötesII	MW	60	−3.1	4.5×10^3	9
WillmanI	MW	38	−2.5	2.6×10^3	10

References.—(1) de Jong et al. 2008; (2) Zucker et al. 2006b, Martin et al. 2008; (3) Martin et al. 2006; (4) Belokurov et al. 2007; (5) Belokurov et al. 2006, Siegel 2006; (6) Simon & Geha 2007; (7) Liu et al. 2008; (8) Zucker et al. 2006a; (9) Walsh et al. 2007; (10) Willman et al. 2006, Siegel 2006.
Notes.—M_* is estimated assuming $M_*/L_V = 3\,{\rm M}_\odot/{\rm L}_\odot$, with L_V determined from M_V quoted in the references. Satellites of MW are discovered by the SDSS, satellites of M31 by the MegaCam survey. Satellite-to-host radii, $r_{\rm host}$, for AndXI, AndXII, & AndXIII are derived using their projected distances from M31, assuming $d_{\rm M31} = 785$ kpc (McConnachie et al. 2005).

and are hosted by dark matter halos with a wide range of masses. In fact, galaxies with the highest fraction of stellar mass built in starbursts are typically old, with τ between 10 and 12 Gyr. Starbursts are not very important overall – 91% of the dwarfs have less than 10% of their stellar mass formed in the starburst mode. Also, we have varied the two parameters describing the starburst mode (the minimum required tidal force and the fraction of gas converted into stars) and found that it has little effect on the SFH distributions.

It should also be mentioned that there does seem to be a trend, at $z = 0$, for the anomalously young dwarf halos to be more massive than the other, more typical, dwarf halos in the model – observationally speaking, these dwarfs would have higher dynamical mass-to-light ratios. Interestingly, at the end of reionization these anomalous dwarfs are hosted by halos with a very wide range of masses, so that there is significant dynamical evolution from the epoch of reionization until the present day. In other words, the younger dwarfs really do have rather "tumultuous" lives.

6. PROJECTIONS FOR LOW-MASS DWARFS

Given the amazing rate of recent discoveries of the population of ultrafaint dwarfs in the SDSS and MegaCam surveys, there stands a challenge to predict the yet-to-be-observed star formation properties of these objects. Our models should in principle be able to predict the mean age and stellar masses for the low-mass dwarfs, however current predictions are not satisfactory.

Figure 7 shows our fiducial model (with the stochasticity parameter $\epsilon_* = 0.1$) extended to masses as low as $M_* = 5 \times 10^3$ M$_\odot$. This model reproduces most closely the observed SFHs of the higher-mass dwarfs, but at $M_* < 5 \times 10^5$ $M_\odot$, it predicts only a modest increase in the number of galaxies. The thick dashed line in Fig. 7 shows the currently-known number of ultrafaint dwarfs, listed in Table 8. The model predictions actually agree very well with the observed number and with the gentle slope of the mass function.

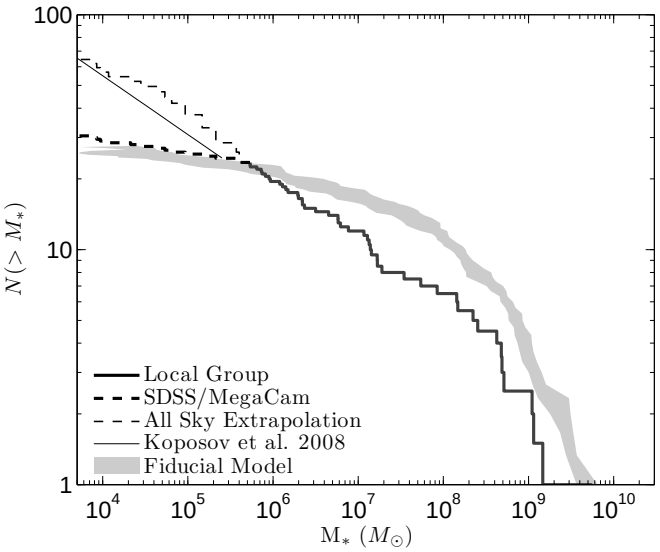

Fig. 7.— The stellar mass function per host halo, extended down to 5×10^3 M$_\odot$. All dwarfs in our fiducial model at $d < 1\,h^{-1}$ Mpc are shown in gray. The Local Group data for $M_* > 5 \times 10^5$ M$_\odot$ are shown with a thick solid line, while the thick dashed line shows the number of presently-known low mass ($M_* < 5 \times 10^5$ M$_\odot$) dwarfs (all the SDSS and MegaCam dwarfs listed in Table 8). The thin dashed line is a likely extrapolation of the mass function to all sky, to account for the incompleteness of current surveys. Thin solid line is an estimate of the luminosity function by Koposov et al. (2008), assuming $M_*/L_V = 3$.

The problem, though, is that the SDSS data release 5, where the bulk of the new dwarfs have been discovered, covers only 20% of the sky. Therefore, we might expect the full sky to contain 5 times as many yet-to-be-discovered ultrafaint dwarfs (Simon & Geha 2007). For the MegaCam survey, the incompleteness factor is even larger, ~ 9 (Martin et al. 2006). Extrapolation to all sky, by multiplying the observed number of dwarfs by these correction factors, is shown by the thin dashed line in Fig. 7. Our model falls well below this corrected mass function.

Koposov et al. (2008) calculate the expected luminosity function of the faint dwarfs more accurately, by estimating the maximum accessible volume of the survey. They conclude that the luminosity function should rise as $dN/dM_V \propto 10^{0.1 M_V}$, which for a fixed mass-to-light ratio results in $N(>M_*) \propto M_*^{-0.25}$. This estimate is also plotted by a straight line in Fig. 7. It lies below our first naive estimate but still significantly above the range of the model. Both incompleteness corrections predict over 50 satellites above 10^4 M$_\odot$, a factor of two larger than in the model. Plus, more dwarfs may remain undetected at larger distances than those probed by the current surveys (~ 300 kpc).

The discrepancy at low mass persists for all variants of our model and we were unable to find a set of pa-

rameters which adequately reproduced the stellar mass function at $M_* > 5 \times 10^5$ M$_\odot$ while predicting appreciable numbers of $M_* < 5 \times 10^5$ M$_\odot$ objects. This rather striking result is evidence that our models are not capturing some critical aspects of the formation of very low mass galaxies. The most naive solutions of significantly reducing either the threshold $\Sigma_{\rm th}$ or the disk structure factor c in eq. (2), thereby allowing a larger portion of gas to participate in star formation, are not viable options since these modifications invariably overpredict the number of $M_* > 5 \times 10^5$ M$_\odot$ dwarfs. In other words, lowering the density threshold produces so many dwarfs that the "missing satellites" are no longer missing and we are once again left with the expectation that we should see in the sky $\sim$ 75 or more luminous dwarf galaxies around the Milky Way, whereas we only observe $\sim$ 30. Kang (2008) also reports a deficit of ultra-faint dwarfs from an independently-developed semi-analytical model of galaxy formation applied to a different collisionless N-body simulation and using the same cosmic reionization model employed here.

Observationally, a new interesting puzzle for our understanding of dwarf galaxy formation is presented by Ryan-Weber et al. (2008). In that study they observe the HI emission from Leo T, the only ultrafaint dwarf with measurable gas content and recent star formation. Based on the density and temperature of HI gas and velocity dispersion of stars, they find that the gas is everywhere globally Jeans-stable, whereas the observed pockets of blue, 200 Myr-old stars indicate continuous star formation. The observed peak of HI column density is a few M$_\odot$ pc^{-2}, close to the star formation threshold. Leo T may thus present another example of stochastic star formation in a handful of isolated molecular clouds, surrounded by largely inert atomic gas. Another relatively massive dwarf, Canes Venatici I, also shows a small fraction of relatively young ($\sim$ 2 Gyr), more metal-rich stars in addition to the predominantly old ($\sim$ 12 Gyr), metal-poor population (Martin et al. 2008). Thus even the ultrafaint dwarfs may, in the future, reveal complex, extended star formation histories.

7. CONCLUSIONS AND DISCUSSION

We have presented phenomenological models for star formation histories of dwarf galaxies in the Local Group, based on the mass assembly histories in cosmological simulations and the stochastic density threshold in Kennicutt-Schmidt law of star formation. Our main conclusions are as follows:

• Models with a stochastic star formation threshold are much more successful than non-stochastic models, such as KGK04, in reproducing the observed star formation histories of the Local Group dwarfs. While the KGK04 model predicted 95% of luminous dwarfs without any recent ($t < 1$ Gyr ago) star formation, our fiducial stochastic model correctly predicts that most dwarfs form a few percent of their stellar mass at late times, in agreement with the recent star formation fraction inferred for the Local Group dwarfs (see Table 1, f_{1G} column and Fig. 1). Stochasticity allows star formation to proceed in isolated regions at late times if the threshold decreases.

• Despite significant improvements of the stochastic model, a some discrepancies with the data remain. (1) Total stellar masses are typically too large by a factor of several. This is a generic problem of both the fixed-threshold and stochastic models presented here. (2) About 10% of the dwarfs in both fixed-threshold and stochastic models have anomalously young stellar populations. These objects build the bulk of their stellar mass in the last 10 Gyr, whereas all of the observed dwarfs contain at least 15% of stars older than 10 Gyr. These young stellar populations in the models are not created only by tidally-induced starbursts, but rather represent late mass assembly of some of the larger satellites.

• Relaxing several model assumptions does not significantly alter these predictions. We have considered the following variants of the fiducial model: allowing late gas accretion within the virial radius of the host halo; different slopes of the star formation law; extended epoch of reionization; and different prescriptions for the photoevaporation of gas from low-mass halos after reionization. All of these variants predict statistically similar observables to the fiducial model.

• A variant of the fiducial model that rejects dwarfs with no star formation in the first 1 or 2 Gyr after the Big Bang significantly improves the f_{10G} stellar fraction. Even though we do not yet have an adequate justification for such a cut, this model predicts the f_{10G}-distribution fully consistent with the Local Group data. Stellar masses, however, are still overestimated.

• Our fiducial model predicts only a modest population of dwarfs with $M_* \lesssim 10^5\,$M$_\odot$, such as those recently discovered by SDSS and the MegaCam survey. The predicted stellar mass function would be an underestimate if the observed numbers are extrapolated to all sky. However, our mass function is still consistent with the presently known dwarfs.

Our phenomenological model contains several free parameters, which allows significant freedom in the range of predicted properties of the satellite galaxies. As we discuss in §3.1, a combination of the parameters, c and $\Sigma_{\rm th0}$, is well constrained by the observed number of dwarfs. Other parameters of the model, apart from the stochasticity ϵ_* which strongly affects late-time star formation, lead only to small and relatively insignificant varations from the fiducial model.

This analytical prescription for star formation is applied to the mass assembly histories of the halos in the cosmological N-body simulation. Since we average over three host halos, our results should not depend significantly on a particular host-halo merger history. Also, by construction all the massive satellite halos that become galaxies in our model survive tidal disruption in the host halo, so that their total number is predicted robustly even if their mass after tidal stripping may depend on the particulars of the simulation.

We should emphasize that our model is not a unique interpretation of the SFH data. Our inferences here neccesarily depend on the assumptions of a Schmidt law of star formation and an exponential profile for the gas density distribution inside dwarf halos as well as the assumptions we have made with the minimum density threshold for star formation, $\Sigma_{\rm th}$. With this latter part of the model we have found that both stochasticity in this threshold over time (§4) and a monotonically decreasing function (§5.4) can lead to extended SFHs – the feature missing from the KGK04 model.

We have assumed in our model that the gas clouds moving on circular orbits should generally remain at the same distance from the galaxy center. However, during mergers and tidal interactions the angular momentum of the gas can be perturbed, leading to radial infall. Such inflow of gas may bring the central gas density above the threshold in some halos soon after the Big Bang and lead to more early star formation. Modeling this process would be very interesting, as it may provide a nice solution for the f_{10G} problem, but the complexity of such a process is beyond our simple model and requires a detailed hydrodynamic simulation.

Additionally, we have not considered any gas outflows due to the radiative and thermal feedback of young stars. Such processes could reduce the amount of available gas supply and the total stellar mass of the simulated dwarfs, which may lead to a closer agreement of the predicted and observed stellar mass function. However, given the uncertainty in the evolution of the gas density profile, we cannot conclude that such feedback is required to reconcile the stellar masses. In fact, from Figure 7 we see that in very low mass halos, where feedback is expected to be stronger, our model needs a boost, rather than a reduction, of star formation. The actual complex details of the condensation of molecular clouds in dwarf halos, which lead to the formation of stars, may turn out more important than the feedback of the stars after their formation.

In spite of these uncertainties, the conclusion we would like to draw from our investigation is that the complex and extended SFHs of the Local Group dwarfs are generally consistent with the expected star formation in cold dark matter halos, and that this star formation is generally governed by the (low) efficiency of conversion of atomic gas into molecular clouds.

We thank Andrew Cole for useful comments on the LMC star formation data, and Andrey Kravtsov and Todd Thompson for helpful suggestions. CO thanks the Ohio State University Center for Cosmology and AstroParticle Physics for its support. OG is supported by the NSF grant AST-0708087.

REFERENCES

Belokurov et al. 2006, ApJ, 647, L111
—. 2007, ApJ, 654, 897
Boissier, S., Prantzos, N., Boselli, A., & Gavazzi, G. 2003, MNRAS, 346, 1215
Butler, D. J., Martínez-Delgado, D., Rix, H.-W., Peñarrubia, J., & de Jong, J. T. A. 2007, AJ, 133, 2274
Chernoff, D. F. & Weinberg, M. D. 1990, ApJ, 351, 121
Cole, A. A., Skillman, E. D., Tolstoy, E., Gallagher, III, J. S., Aparicio, A., Dolphin, A. E., Gallart, C., Hidalgo, S. L., Saha, A., Stetson, P. B., & Weisz, D. R. 2007, ApJ, 659, L17
Colín, P., Avila-Reese, V., & Valenzuela, O. 2000, ApJ, 542, 622
Crain, R. A., Eke, V. R., Frenk, C. S., Jenkins, A., McCarthy, I. G., Navarro, J. F., & Pearce, F. R. 2007, MNRAS, 377, 41
de Jong, J. T. A., et al. 2008, ApJ, 680, 1112
Dekel, A. & Silk, J. 1986, ApJ, 303, 39
Dekel, A. & Woo, J. 2003, MNRAS, 344, 1131
Dolphin, A. E. 2002, MNRAS, 332, 91
Dolphin, A. E., Weisz, D. R., Skillman, E. D., & Holtzman, J. A. 2005, preprint (astro-ph/0506430)
Fisher, J. R. & Tully, R. B. 1975, A&A, 44, 151
Geha, M., Blanton, M. R., Masjedi, M., & West, A. A. 2006, ApJ, 653, 240
Gnedin, N. Y. 2000, ApJ, 542, 535
Grebel, E. K., Gallagher, III, J. S., & Harbeck, D. 2003, AJ, 125, 1926
Harris, J. & Zaritsky, D. 2004, AJ, 127, 1531
Hernandez, X., Park, C., Cervantes-Sodi, B., & Choi, Y.-Y. 2007, MNRAS, 375, 163
Heyer, M. H., Corbelli, E., Schneider, S. E., & Young, J. S. 2004, ApJ, 602, 723
Hoeft, M., Yepes, G., & Gottloeber, S. 2007, preprint (arXiv:0708.0229)
Holtzman, J. A., Afonso, C., & Dolphin, A. 2006, ApJS, 166, 534
Hurley, J. R., Pols, O. R., & Tout, C. A. 2000, MNRAS, 315, 543
Ibata, R., Martin, N. F., Irwin, M., Chapman, S., Ferguson, A. M. N., Lewis, G. F., & McConnachie, A. W. 2007, ApJ, 671, 1591
Irwin, M. J., Ferguson, A. M. N., Huxor, A. P., Tanvir, N. R., Ibata, R. A., & Lewis, G. F. 2008, ApJ, 676, L17
Irwin et al. 2007, ApJ, 656, L13
Kamionkowski, M. & Liddle, A. R. 2000, Physical Review Letters, 84, 4525
Kang, X. 2008, ArXiv e-prints (arXiv:0806.3279)
Kauffmann, G., White, S. D. M., & Guiderdoni, B. 1993, MNRAS, 264, 201
Kaufmann, T., Wheeler, C., & Bullock, J. S. 2007, MNRAS, 382, 1187
Kennicutt, Jr., R. C. 1998, ApJ, 498, 541
Klypin, A., Kravtsov, A. V., Valenzuela, O., & Prada, F. 1999, ApJ, 522, 82
Komatsu, E., Dunkley, J., Nolta, M. R., Bennett, C. L., Gold, B., Hinshaw, G., Jarosik, N., Larson, D., Limon, M., Page, L., Spergel, D. N., Halpern, M., Hill, R. S., Kogut, A., Meyer, S. S., Tucker, G. S., Weiland, J. L., Wollack, E., & Wright, E. L. 2008, ApJS, submitted (arXiv:0803.0547)
Koposov, S., Belokurov, V., Evans, N. W., Hewett, P. C., Irwin, M. J., Gilmore, G., Zucker, D. B., Rix, H. ., Fellhauer, M., Bell, E. F., & Glushkova, E. V. 2008, ApJaccepted (arXiv:0706.2687)
Kopylov, A. I., Tikhonov, N. A., Fabrika, S., Drozdovsky, I., & Valeev, A. F. 2008, MNRAS, 387, L45
Kravtsov, A. V. & Gnedin, O. Y. 2005, ApJ, 623, 650
Kravtsov, A. V., Gnedin, O. Y., & Klypin, A. A. 2004, ApJ, 609, 482
Kroupa, P. 2001, MNRAS, 322, 231
Lee, H., Skillman, E. D., Cannon, J. M., Jackson, D. C., Gehrz, R. D., Polomski, E. F., & Woodward, C. E. 2006, ApJ, 647, 970
Liu, C., Hu, J., Newberg, H., & Zhao, Y. 2008, A&A, 477, 139
Madau, P., Diemand, J., & Kuhlen, M. 2008, ApJ, 679, 1260
Majewski, S. R., Beaton, R. L., Patterson, R. J., Kalirai, J. S., Geha, M. C., Muñoz, R. R., Seigar, M. S., Guhathakurta, P., Gilbert, K. M., Rich, R. M., Bullock, J. S., & Reitzel, D. B. 2007, ApJ, 670, L9
Martin, N. F., Coleman, M. G., De Jong, J. T. A., Rix, H.-W., Bell, E. F., Sand, D. J., Hill, J. M., Thompson, D., Burwitz, V., Giallongo, E., Ragazzoni, R., Diolaiti, E., Gasparo, F., Grazian, A., Pedichini, F., & Bechtold, J. 2008, ApJ, 672, L13
Martin, N. F., Ibata, R. A., Bellazzini, M., Irwin, M. J., Lewis, G. F., & Dehnen, W. 2004, MNRAS, 348, 12
Martin, N. F., Ibata, R. A., Irwin, M. J., Chapman, S., Lewis, G. F., Ferguson, A. M. N., Tanvir, N., & McConnachie, A. W. 2006, MNRAS, 371, 1983
Mateo, M. L. 1998, ARA&A, 36, 435
McConnachie, A. W., Irwin, M. J., Ferguson, A. M. N., Ibata, R. A., Lewis, G. F., & Tanvir, N. 2004, MNRAS, 350, 243
—. 2005, MNRAS, 356, 979
McKee, C. F. & Ostriker, E. C. 2007, ARA&A, 45, 565
Moore, B., Ghigna, S., Governato, F., Lake, G., Quinn, T., Stadel, J., & Tozzi, P. 1999, ApJ, 524, L19
Prieto, J. L. & Gnedin, O. Y. 2006, ArXiv Astrophysics e-prints, preprint (astro-ph/0608069)
Ricotti, M. & Gnedin, N. Y. 2005, ApJ, 629, 259
Robertson, B. E., & Kravtsov, A. V. 2008, ApJ, 680, 1083
Ryan-Weber, E. V., Begum, A., Oosterloo, T., Pal, S., Irwin, M. J., Belokurov, V., Evans, N. W., & Zucker, D. B. 2008, MNRAS, 384, 535
Siegel, M. H. 2006, ApJ, 649, L83
Simon, J. D. & Geha, M. 2007, ApJ, 670, 313

Smecker-Hane, T. A., Cole, A. A., Gallagher, III, J. S., & Stetson, P. B. 2002, ApJ, 566, 239
Spergel, D. N. & Steinhardt, P. J. 2000, Physical Review Letters, 84, 3760
Tassis, K., Kravtsov, A. V., & Gnedin, N. Y. 2008, ApJ, 672, 888
Thilker et al. 2007, ApJS, 173, 538
Thoul, A. A. & Weinberg, D. H. 1996, ApJ, 465, 608
Vitvitska, M., Klypin, A. A., Kravtsov, A. V., Wechsler, R. H., Primack, J. R., & Bullock, J. S. 2002, ApJ, 581, 799
Walsh, S. M., Jerjen, H., & Willman, B. 2007, ApJ, 662, L83
Willman, B., Masjedi, M., Hogg, D. W., Dalcanton, J. J., Martinez-Delgado, D., Blanton, M., West, A. A., Dotter, A., & Chaboyer, B. 2006, preprint (astro-ph/0603486)
Willman et al. 2005a, AJ, 129, 2692
—. 2005b, ApJ, 626, L85
Zentner, A. R. & Bullock, J. S. 2003a, in American Institute of Physics Conference Series, Vol. 666, The Emergence of Cosmic Structure, ed. S. H. Holt & C. S. Reynolds, 151–154
Zentner, A. R. & Bullock, J. S. 2003b, ApJ, 598, 49
Zucker et al. 2004, ApJ, 612, L121
—. 2006a, ApJ, 650, L41
—. 2006b, ApJ, 643, L103
—. 2007, ApJ, 659, L21